ELSEVIER

Elastodynamic Green's function for reinforced concrete beams

M.R. Chitnis [a,1], Y.M. Desai [a,*], A.H. Shah [b], T. Kant [a]

[a] *Department of Civil Engineering, Indian Institute of Technology Bombay, Powai, Mumbai 400 076, India*
[b] *Department of Civil Engineering, University of Manitoba, Winnipeg, MB, Canada R3T 5V6*

Abstract

A semi-analytical solution procedure for three dimensional wave propagation in reinforced concrete (RC) beams has been presented in this paper. Elastodynamic Green's function has been derived by employing the compatibility conditions and utilizing the symmetry conditions at the loaded cross section. Numerical procedure developed for the Green's function has been validated using results available in the literature for an infinite laminated composite plate. Three-dimensional wave propagation analysis has been performed for reinforced concrete beam sections of T and L shapes which are common forms of structural elements. Steel reinforcement has been modeled in the finite element mesh. Effect of corrosion has also been included in the finite element model. Green's function for reinforced concrete sections affected by corrosion of steel unit normalized frequency has been evaluated for illustration. Accuracy of the solution technique has been evaluated in terms of the percentage error in energy balance between the input energy of the applied unit load and the output energy carried by the propagating wave modes. The percentage error has been found to be negligible in all the cases considered here. A simple and accurate numerical method has been presented here as a tool to evaluate Green's function for RC beams and can be used to detect corrosion.
© 2005 Elsevier Ltd. All rights reserved.

Keywords: Wave propagation; Green's function; Reinforced concrete beam; Corrosion

1. Introduction

Reinforced concrete (RC) beams are commonly used structural elements in Civil Engineering infrastructures. A suitable strategy is desired to monitor their structural integrity for safety of infrastructures under

---

* Corresponding author. Tel.: +91 2576 4349; fax: +91 2576 7302.
  E-mail addresses: mrchitnis@iitb.ac.in (M.R. Chitnis), desai@civil.iitb.ac.in (Y.M. Desai).
[1] Tel.: +91 022 2576 7333/7301; fax: +91 022 2576 7302

operating environment. One essential component of a monitoring strategy is to include technique for detecting and characterizing flaws such as cracks and corrosions.

Green's function can be advantageously employed in quantitative nondestructive evaluation (QNDE) for locating and estimating the size and extent of flaws. Green's function provides the loading function on flaws if hybrid formulation is pursued. It also constitutes the kernel of the boundary integral in boundary element method. Green's function is constructed through the summation of wave modes (spectral data). Spectral data is obtained through wave propagation analysis.

Wave propagation in layered anisotropic media has been investigated in the past using different approaches. Datta et al. (1988) presented a stiffness method to analyze dispersive wave propagation in a laminated anisotropic plate. The lamina was divided into several sub-layers and displacement distribution through the thickness of each layer was approximated by a polynomial function. Liu et al. (1990) presented a numerical method to investigate harmonic wave propagation in anisotropic laminated strips in which displacement field within each element was approximated by a linear expansion in the thickness direction and by a series expansion in the width direction. Karunasena et al. (1991) developed an analytical method to derive dispersion equation for guided waves in anisotropic plate by using propagator matrix approach. The method was found to be mathematically cumbersome and time consuming as compared to the stiffness approach developed earlier. Chimenti (1997) reviewed number of experimental and theoretical works in the field of ultrasonic characterization of materials using guided waves in plate-like structures. Most investigations in the field of wave propagation and scattering of guided ultrasonic waves in laminated fiber reinforced plates considered plates of large in-plane dimensions and thus essentially two-dimensional situations were investigated. However, Taweel et al. (2000) and Mukdadi et al. (2002) have attempted to analyze propagation of waves in fiber reinforced laminated plates of finite width, by considering the three-dimensional effect, and by using a semi analytical finite element method. Deformation of the cross section was modeled by two-dimensional finite elements and analytical representation of propagating waves along the length of the plate was used.

Zhu et al. (1995) investigated two-dimensional Green's functions for a laminated plate by a modal representation approach. Liu and Lam (1996) developed an exact matrix formulation for a two-dimensional time-harmonic elastodynamic Green's functions for anisotropic media. Displacements and stresses were expressed in the Fourier transform domain with help of modal expansion. Zhuang et al. (1999) presented Green's function for a laminated anisotropic circular cylinder formed by superposing modal solutions generated from a system of equations based on semianalytical finite element formulation.

Green and Green (2000) presented a computational method for wave propagation due to a point load in composite plates and laminates in which integral transforms were used to reduce governing equations. Mal (2002) analyzed elastic waves generated by a localized dynamic source in structural composites. External as well as internal localized dynamic sources were considered. A low-velocity foreign object impact was considered under external type and sudden initiation of crack and its rapid growth was considered under the internal category. Cavigila and Morro (2000) investigated time-harmonic wave propagation in multilayers consisting of a sequence of inhomogeneous layers separated by discontinuity surfaces. A wave-splitting procedure was applied based on the use of the eigenvectors of the matrix associated with the system.

Two methodologies are possible to construct steady-state Green's function using spectral data (Zhuang et al., 1999). One is based on integral transform and the other on forced vibration. Recently, Mukdadi and Datta (2003) constructed the Green's function based on integral transform. Other approach of forced vibration has been pursued in the present work by making use of the spectral data obtained using three dimensional wave propagation analysis (Taweel et al., 2000). The dispersion equation has been solved using three-dimensional semi analytical method in which eight-node or nine-node isoparametric elements are used to model cross section of a beam and an exponential function is used to define displacement field along length of the beam. Symmetry conditions at the loaded cross section have been advantageously employed to construct steady-state elastodynamic Green's function for a beam of arbitrary cross section. Method has

been applied to practical problems in Civil Engineering field of reinforced concrete L and T beams. Parametric investigation has been performed to identify finite element mesh size required to obtain converged solution for reinforced concrete beams. Converged eigenvalues and eigenmodes obtained from wave propagation analysis for a particular frequency have been utilized to evaluate displacement field in Green's function. For reinforced concrete beam affected by corrosion of steel, two layers of steel rust and degenerated concrete around each steel bar have been modeled separately. Effect of corrosion of steel reinforcement has been investigated by comparing displacement variation curves for corroded section of reinforced concrete beams with those for original reinforced concrete beams.

2. Theoretical formulation

2.1. Wave propagation in reinforced concrete beam

Consider a time-harmonic elastic wave passing through a reinforced concrete beam. Direction of propagation of wave is assumed to be along the longitudinal axis of the beam. For simplicity in numerical modeling, stirrups and bends in reinforced concrete beam have been neglected and it is assumed to consist of reinforcement bars in the longitudinal direction. The global coordinate system (X, Y, Z) as shown in Fig. 1(a) is adopted to model the beam. A semi-analytical numerical solution technique is adopted to analyze wave propagation in a reinforced concrete beam. The cross section has been modeled with nine-node isoparametric quadrilateral elements and the wave motion along longitudinal axis is defined with analytical expression.

Displacement field inside an element comprising of 'n' number of nodes can be expressed as

$$\mathbf{u}(x,y,z,t) = \left\{ \begin{array}{c} u(x,y,z,t) \\ v(x,y,z,t) \\ w(x,y,z,t) \end{array} \right\} = \left\{ \begin{array}{c} \sum_{i=1}^{n} N_i(y,z)u_i(x,t) \\ \sum_{i=1}^{n} N_i(y,z)v_i(x,t) \\ \sum_{i=1}^{n} N_i(y,z)w_i(x,t) \end{array} \right\} = \mathbf{Nd} \tag{1}$$

where

$$\mathbf{N} = \mathbf{N}(y,z); \quad \mathbf{d} = \mathbf{d}(x,t)$$

are the element shape matrix of size $3 \times 3n$ and displacement vector of size *3n*, respectively.

Rearranging the terms node-wise, displacement field can be written as

$$\mathbf{u} = \mathbf{Nd} = \begin{bmatrix} N_1 & 0 & 0 & \cdots & N_j & 0 & 0 & \cdots & N_n & 0 & 0 \\ 0 & N_1 & 0 & \cdots & 0 & N_j & 0 & \cdots & 0 & N_n & 0 \\ 0 & 0 & N_1 & \cdots & 0 & 0 & N_j & \cdots & 0 & 0 & N_n \end{bmatrix} \left\{ \begin{array}{c} \mathbf{d}_1 \\ \vdots \\ \mathbf{d}_j \\ \vdots \\ \mathbf{d}_n \end{array} \right\} \tag{2}$$

where

$$\mathbf{d}_j^{\mathrm{T}} = \{ u_j \quad v_j \quad w_j \}$$

represents the nodal displacement vector corresponding to node number *j*.

The strain–displacement relation is expressed in a split operator form

$$\boldsymbol{\varepsilon} = \mathbf{Lu} = (\mathbf{L}_{yz} + \mathbf{L}_x)\mathbf{u} \tag{3}$$
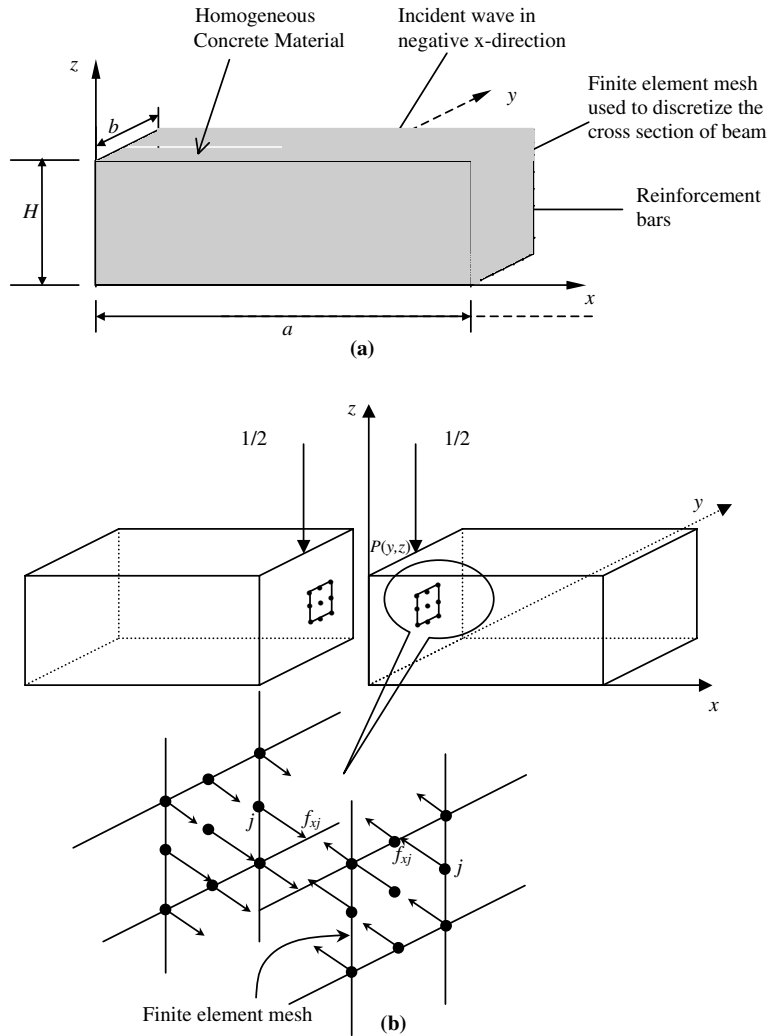
Fig. 1. Three-dimensional Green's function for laminated composite beam (a) Geometry, co-ordinate axes and finite element model; (b) Symmetry conditions over the cross section of beam at $x = 0$.

Here

$$\boldsymbol{\varepsilon} = \left\{ \varepsilon_x \quad \varepsilon_y \quad \varepsilon_z \quad \gamma_{yz} \quad \gamma_{xz} \quad \gamma_{xy} \right\}^{\mathrm{T}} \tag{4}$$

$$\mathbf{L}_{yz}^{\mathrm{T}} = \begin{bmatrix} 0 & 0 & 0 & 0 & \dfrac{\partial}{\partial z} & \dfrac{\partial}{\partial y} \\ 0 & \dfrac{\partial}{\partial y} & 0 & \dfrac{\partial}{\partial z} & 0 & 0 \\ 0 & 0 & \dfrac{\partial}{\partial z} & \dfrac{\partial}{\partial y} & 0 & 0 \end{bmatrix}, \quad \mathbf{L}_x^{\mathrm{T}} = \begin{bmatrix} \dfrac{\partial}{\partial x} & 0 & 0 & 0 & 0 & 0 \\ 0 & 0 & 0 & 0 & 0 & \dfrac{\partial}{\partial x} \\ 0 & 0 & 0 & 0 & \dfrac{\partial}{\partial x} & 0 \end{bmatrix} \tag{5}$$

Substituting for the displacement vector **u** from Eqs. (2) and (3) can be shown to be

$$\boldsymbol{\varepsilon} = \mathbf{L}_{yz}\mathbf{N}\mathbf{d} + \mathbf{L}_x\mathbf{N}\mathbf{d} = \mathbf{b}_1\mathbf{d} + \mathbf{b}_2\mathbf{d}_{,x} \tag{6}$$

where

$$\mathbf{b}_1^{\mathrm{T}} = \begin{bmatrix} 0 & 0 & 0 & 0 & N_{1,z} & N_{,y} \\ 0 & N_{1,y} & 0 & 0 & N_{1,z} & 0 \\ 0 & 0 & N_{1,z} & N_{1,y} & 0 & 0 \\ . & . & . & . & . & . \\ . & . & . & . & . & . \\ 0 & 0 & 0 & 0 & N_{j,z} & N_{j,y} \\ 0 & N_{j,y} & 0 & 0 & N_{j,z} & 0 \\ 0 & 0 & N_{j,z} & N_{j,y} & 0 & 0 \\ . & . & . & . & . & . \\ . & . & . & . & . & . \\ 0 & 0 & 0 & 0 & N_{n,z} & N_{n,y} \\ 0 & N_{n,y} & 0 & 0 & N_{n,z} & 0 \\ 0 & 0 & N_{n,z} & N_{n,y} & 0 & 0 \end{bmatrix}_{(3n\times6)} ; \quad \mathbf{b}_2^{\mathrm{T}} = \begin{bmatrix} N_1 & 0 & 0 & 0 & 0 & 0 \\ 0 & 0 & 0 & 0 & 0 & N_1 \\ 0 & 0 & 0 & 0 & N_1 & 0 \\ . & . & . & . & . & . \\ . & . & . & . & . & . \\ N_j & 0 & 0 & 0 & 0 & 0 \\ 0 & 0 & 0 & 0 & 0 & N_j \\ 0 & 0 & 0 & 0 & N_j & 0 \\ . & . & . & . & . & . \\ . & . & . & . & . & . \\ N_n & 0 & 0 & 0 & 0 & 0 \\ 0 & 0 & 0 & 0 & 0 & N_n \\ 0 & 0 & 0 & 0 & N_n & 0 \end{bmatrix}_{(3n\times6)} ;$$

and

$$\mathbf{d}_{,x} = \frac{\partial \mathbf{d}}{\partial x} \tag{7}$$

The constitutive relation for each distinct material comprising the cross section can be written as

$$\boldsymbol{\sigma} = \mathbf{C}\boldsymbol{\varepsilon} \tag{8}$$

where

$$\boldsymbol{\sigma} = \{ \sigma_x \quad \sigma_y \quad \sigma_z \quad \tau_{yz} \quad \tau_{xz} \quad \tau_{xy} \}^{\mathrm{T}} \tag{9}$$

and $\mathbf{C}$ is a (6×6) matrix of anisotropic elastic moduli.

The governing equations of motion for a beam can be derived by using Hamilton's principle

$$\delta \int_{t_1}^{t_2} \{ T - (U + V_E) \} \, \mathrm{d}t = 0 \tag{10}$$

Here T is the kinetic energy. On the other hand, U and V_E represent the internal strain energy and potential energy due to external forces, respectively. The kinetic energy in terms of the velocity vector $\mathbf{u}$ and unit mass density ρ can be shown in the form

$$T = \frac{1}{2} \int_V \dot{\mathbf{u}}^T \boldsymbol{\rho} \dot{\mathbf{u}} \, \mathrm{d}v \tag{11}$$

where

$$\boldsymbol{\rho} = \begin{bmatrix} \rho & 0 & 0 \\ 0 & \rho & 0 \\ 0 & 0 & \rho \end{bmatrix}$$

is the mass matrix.

The strain energy U is represented by

$$U = \frac{1}{2} \int_V \boldsymbol{\varepsilon}^T \mathbf{C}\boldsymbol{\varepsilon} \, \mathrm{d}v \tag{12}$$

The potential energy V_E consists of applied traction on some generic cross-section and it is expressed as

$$V_E = \frac{1}{2} \int_A \mathbf{u}^T \boldsymbol{\sigma}_\mathrm{f} \, dA \tag{13}$$

Here $\boldsymbol{\sigma}_\mathrm{f}$ denotes the normal and the shear tractions on the cross-sectional surface.

Substituting Eqs. (2) and (6) into Eqs. (11)–(13), and using Eq. (10),

$$\delta \int_{t_1}^{t_2} \left[\int_V \left(\dot{\mathbf{d}}^\mathrm{T} \mathbf{N}^\mathrm{T} \rho \mathbf{N} \dot{\mathbf{d}} - \mathbf{d}^\mathrm{T} \mathbf{b}_1^\mathrm{T} \mathbf{C} \mathbf{b}_1 \mathbf{d} - \mathbf{d}^\mathrm{T} \mathbf{b}_1^\mathrm{T} \mathbf{C} \mathbf{b}_2 \mathbf{d}_{,x} - \mathbf{d}_{,x}^\mathrm{T} \mathbf{b}_2^\mathrm{T} \mathbf{C} \mathbf{b}_1 \mathbf{d} - \mathbf{d}_{,x}^\mathrm{T} \mathbf{b}_2^\mathrm{T} \mathbf{C} \mathbf{b}_2 \mathbf{d}_{,x} \right) dx\,dy\,dz \right.$$
$$\left. + \int_S \left(\mathbf{d}^\mathrm{T} \mathbf{N}^\mathrm{T} \boldsymbol{\sigma}_f \right) dy\,dz \right] dt = 0 \tag{14}$$

can be obtained.

By performing the integration over area of cross-section of the element,

$$\delta \int_{t_1}^{t_2} \frac{1}{2} \left[\int \left(\dot{\mathbf{d}}^\mathrm{T} \mathbf{m} \dot{\mathbf{d}} - \mathbf{d}^\mathrm{T} \mathbf{k}_{11} \mathbf{d} - \mathbf{d}^\mathrm{T} \mathbf{k}_{12} \mathbf{d}_{,x} - \mathbf{d}_{,x}^\mathrm{T} \mathbf{k}_{21} \mathbf{d} - \mathbf{d}_{,x}^\mathrm{T} \mathbf{k}_{22} \mathbf{d}_{,x} \right) dx + \mathbf{d}^\mathrm{T} \mathbf{f} \right] dt = 0 \tag{15}$$

is formed, where

$$\mathbf{k}_{\alpha\beta} = \int_A \mathbf{b}_\alpha^\mathrm{T} \mathbf{C} \mathbf{b}_\beta \, dy\,dz, \alpha, \beta = 1, 2; \quad \mathbf{m} = \int_A \mathbf{N}^\mathrm{T} \boldsymbol{\rho} \mathbf{N} \, dy\,dz \quad \text{and} \quad \mathbf{f} = \int_A \mathbf{N}^\mathrm{T} \boldsymbol{\sigma}_\mathrm{f} \, dy\,dz \tag{16}$$

Eq. (15) can be written for the entire beam by performing assembly of all the matrices defined in Eq. (16) as

$$\delta \int_{t_1}^{t_2} \frac{1}{2} \left[\int \left(\dot{\mathbf{q}}^\mathrm{T} \mathbf{M} \dot{\mathbf{q}} - \mathbf{q}^\mathrm{T} \mathbf{K}_{11} \mathbf{q} - \mathbf{q}^\mathrm{T} \mathbf{K}_{12} \mathbf{q}_{,x} - \mathbf{q}_{,x}^\mathrm{T} \mathbf{K}_{21} \mathbf{q} - \mathbf{q}_{,x}^\mathrm{T} \mathbf{K}_{22} \mathbf{q}_{,x} \right) dx + \mathbf{q}^\mathrm{T} \mathbf{F} \right] dt = 0 \tag{17}$$

where

$$\mathbf{K}_{11} = \sum_{n=1}^{NE} \mathbf{k}_{11n}; \quad \mathbf{K}_{12} = \mathbf{K}_{21}^\mathrm{T} = \sum_{n=1}^{NE} \mathbf{k}_{12n}; \quad \mathbf{K}_{22} = \sum_{n=1}^{NE} \mathbf{k}_{22n}; \quad \mathbf{M} = \sum_{n=1}^{NE} \mathbf{m}_n; \quad \mathbf{F} = \sum_{n=1}^{NE} \mathbf{f}_n \tag{18}$$

and NE represents the total number of elements over the cross-section, and $\mathbf{q}$ is the global displacement vector.

The displacement field for the wave propagation in a reinforced concrete beam can be expressed as

$$\mathbf{q} = \mathbf{q}_0 e^{i(\lambda x - \omega t)} \tag{19}$$

Here ω represents the circular frequency, λ is the complex wave number and $\mathbf{q}_0$ is the vector of nodal displacements at the origin.

Following governing equation can be obtained for propagation of wave by substituting Eq. (19) in Eq. (17), performing the variation and dropping the non-homogeneous part of Eq. (17) and the common exponential term.

$$\left[\mathbf{K}_1 + i\lambda \mathbf{K}_2 + \lambda^2 \mathbf{K}_3 - \omega^2 \mathbf{M} \right] \mathbf{q}_0 = 0 \tag{20}$$

where $\mathbf{K}_1 = \mathbf{K}_{11}, \mathbf{K}_2 = \mathbf{K}_{12} - \mathbf{K}_{21}$ and $\mathbf{K}_3 = \mathbf{K}_{22}$.

The determinant of Eq. (20) yields the dispersion relation for propagation of wave.

Equation for wave propagation in a reinforced concrete beam is written in a compact form as

$$\mathbf{K} - \omega^2 \mathbf{M} = 0 \tag{21}$$

where

$$\mathbf{K} = \mathbf{K}_1 + \mathrm{i}\lambda\mathbf{K}_2 + \lambda^2\mathbf{K}_3$$

For a nontrivial solution, the determinant of the coefficient matrix in Eq. (21) must be zero. This results in a generalized eigenvalue problem when λ is specified. For a bounded solution, the wave travelling in the positive x-direction must correspond to a complex wave number, λ, having a form $\lambda = \lambda_R + \lambda_I$ where λ_R and $\lambda_I \geqslant 0$. In contrast, if $\lambda_R = 0$ and $\lambda_I \neq 0$, the mode is evanescent or non-propagating.

To simplify Eq. (21) mathematically it is written in an expanded matrix form as

$$[\mathbf{A} - \lambda\mathbf{B}]\mathbf{Q} = 0 \tag{22}$$

where

$$\mathbf{A} = \begin{bmatrix} 0 & \mathbf{I} \\ \mathbf{K}_1^* & i\mathbf{K}_2 \end{bmatrix}, \quad \mathbf{B} = \begin{bmatrix} \mathbf{I} & 0 \\ 0 & -\mathbf{K}_3 \end{bmatrix}, \tag{23}$$

$$\mathbf{Q} = \{\, \mathbf{q}_0 \quad \lambda\mathbf{q}_0 \,\}^t \tag{24}$$

and

$$\mathbf{K}_1^* = \mathbf{K}_1 - \omega^2\mathbf{M} \tag{25}$$

A nontrivial solution to Eq. (25) can be sought by setting the determinant of the coefficient matrix to zero. This results in the dispersion relation to solve for the eigenvalues λ for a given value of ω.

2.2. Green's function for a reinforced concrete beam

Consider a concentrated time-harmonic unit load of frequency ω acting at a point $P(y,z)$ in the domain of the reinforced concrete beam as shown in Fig. 1(b). Direction of application of the unit load may coincide with any of the three global co-ordinate axes. However, Green's function for a typical case of unit load acting in z-direction has been discussed in the sequel for illustration. The cross section of the beam is modeled by a finite element mesh, which divides the layers into sub-layers. Since symmetry conditions are employed, only right hand side ($x \geqslant 0$) region of the beam is considered in the analysis.

The displacement vector $\mathbf{q}_x$, at any point in the beam section is approximated by the modal sum of a finite number of modes MS in the form

$$\mathbf{q}_x = \sum_{m=1}^{MS} A_m\mathbf{q}_m\mathrm{e}^{\mathrm{i}\lambda_m x} \tag{26}$$

where A_m is the unknown amplitude of mth mode and

$$\mathbf{q}_m^{\mathrm{T}} = \{\, u_{1m},\ldots, \quad u_{im},\ldots, \quad u_{NNm}, \quad v_{1m},\ldots, \quad v_{im},\ldots, \quad v_{NNm}, \quad w_{1m},\ldots, \quad w_{im},\ldots, \quad w_{NNm} \,\} \tag{27}$$

is the displacement mode shape vector corresponding to the wave number λ_m which has been evaluated using Eq. (22).

The displacement vector at $x = 0$ is expressed as

$$\mathbf{q}_0 = \mathbf{G}\mathbf{A} \tag{28}$$

where

$$\mathbf{G} = [\mathbf{q}_1, \quad \ldots, \quad \mathbf{q}_m, \quad \ldots, \quad \mathbf{q}_{MS}]; \mathbf{A}^{\mathrm{T}} = \{\, A_1, \quad \ldots, \quad A_m, \quad \ldots, \quad A_{MS} \,\} \tag{29}$$

$\mathbf{G}$ is the displacement mode shape matrix of size ($3NN \times MS$) and $\mathbf{A}$ is the amplitude vector of MS dimension. Here NN denotes total number of nodes in the finite element mesh defining the cross section of the beam.

The force vector at $x = 0$ can be formed as

$$\mathbf{f}_0 = \mathbf{FA} \tag{30}$$

where

$$\mathbf{F} = [\mathbf{f}_1, \quad \ldots, \quad \mathbf{f}_m, \quad \ldots, \quad \mathbf{f}_{MS}] \tag{31}$$

and

$$\mathbf{f}_m^T = \{ f_{x1m} \ldots, f_{xim}, \ldots, f_{xNNm} \quad f_{y1m} \ldots, f_{yim}, \ldots, f_{yNNm} \quad f_{z1m} \ldots, f_{zim}, \ldots, f_{zNNm} \} \tag{32}$$

Forces f_{xim}, f_{yim} and f_{zim} are the resultant of stresses σ_x, τ_{xy} and τ_{xz} derived from vector $\mathbf{q}_m$ using strain–displacement and stress–strain relations.

Consider a unit concentrated load acting at a point $P(y, z)$ in the negative z-direction on the top of the beam as shown in Fig. 1(b). Symmetric conditions with respect to vertical plane $x = 0$ lead to following definition of displacement and force mode shape vectors, respectively.

$$\mathbf{q}_0^T = \left\{ \mathbf{0} \Big| \quad \mathbf{q}_{0y}^T \Big| \quad \mathbf{q}_{0z}^T \right\}; \quad \mathbf{f}_0^T = \left\{ \mathbf{f}_{0x}^T \Big| \quad \mathbf{0} \Big| \quad \mathbf{f}_{0z}^T \right\} \tag{33}$$

where

$$\mathbf{0}^T = \{ 0 \ldots, \quad 0 \ldots, \quad 0 \}_{NN}; \quad \mathbf{q}_{0y}^T = \{ v_1 \ldots, \quad v_i \ldots, \quad v_{NN} \}_{NN};$$
$$\mathbf{q}_{0z}^T = \{ w_1 \ldots, \quad w_i \ldots, \quad w_{NN} \}_{NN}; \quad \mathbf{f}_{0x}^T = \{ f_{x1} \ldots, \quad f_{xi} \ldots, \quad f_{xNN} \}_{NN}$$

and

$$\begin{array}{c} \text{Node } L \\ \downarrow \\ \mathbf{f}_{0z}^T = \{ 0 \ldots, \quad -\tfrac{1}{2} \ldots, \quad 0 \}_{NN} \end{array} \tag{34}$$

Node L represented above indicates the particular node in the finite element mesh at which the unit load acts. Thus the term $-1/2$ shown in above equation may occupy any location from 1 to NN in the vector $\mathbf{f}_{0z}$.

By using Eq. (33), Eqs. (28) and (30) can be rewritten as

$$\begin{bmatrix} \mathbf{G}_1 \\ \mathbf{G}_2 \\ \mathbf{G}_3 \end{bmatrix} \mathbf{A} = \left\{ \begin{array}{c} \mathbf{0} \\ \mathbf{q}_{0y} \\ \mathbf{q}_{0z} \end{array} \right\} \tag{35}$$

$$\begin{bmatrix} \mathbf{F}_1 \\ \mathbf{F}_2 \\ \mathbf{F}_3 \end{bmatrix} \mathbf{A} = \left\{ \begin{array}{c} \mathbf{f}_{0x} \\ \mathbf{0} \\ \mathbf{f}_{0z} \end{array} \right\} \tag{36}$$

Here $\mathbf{G}_i$ and $\mathbf{F}_i$ ($i = 1, 2, 3$) are NN by MS matrices.

By combining the first part of Eq. (35) and the last two parts of Eq. (36),

$$\mathbf{HA} = \mathbf{r} \tag{37}$$

is obtained where

$$\mathbf{H} = \begin{bmatrix} \mathbf{G}_1 \\ \mathbf{F}_2 \\ \mathbf{F}_3 \end{bmatrix}; \quad \mathbf{r} = \left\{ \begin{array}{c} \mathbf{0} \\ \mathbf{0} \\ \mathbf{f}_{0z} \end{array} \right\} \tag{38}$$

Matrix $\mathbf{H}$ defined in Eq. (38) is a rectangular matrix and vector $\mathbf{A}$ cannot be evaluated directly from Eq. (37). A variational solution to the problem can be obtained by applying the principle of virtual displacement wherein first variation of work done by forces is minimized. A complementary matrix $\mathbf{H}^-$ described below is formed and both sides of Eq. (37) are pre-multiplied by $\overline{\mathbf{H}}^{-\mathrm{T}}$ to obtain

$$\overline{\mathbf{H}}^{-\mathrm{T}}\mathbf{H}\mathbf{A} = \overline{\mathbf{H}}^{-\mathrm{T}}\mathbf{r} \tag{39}$$

The amplitude coefficients can be obtained from Eq. (39) as

$$\mathbf{A} = \left[\overline{\mathbf{H}}^{-\mathrm{T}}\mathbf{H}\right]^{-1}\overline{\mathbf{H}}^{-\mathrm{T}}\mathbf{r} \tag{40}$$

Here

$$\mathbf{H}^- = \begin{bmatrix} \mathbf{F}_1 \\ \mathbf{G}_2 \\ \mathbf{G}_3 \end{bmatrix} \tag{41}$$

and overbar refers to the complex conjugate.

The input energy in the reinforced concrete beam due to the unit concentrated load (Zhu et al., 1995) can be expressed as

$$I^{\mathrm{in}} = \frac{1}{2}\omega\ \mathrm{Im}[\bar{q}_{\mathrm{p}}] \tag{42}$$

The term q_{p} in the above equation represents the displacement of the loading point in the direction of the unit load. The symbol "Im" used in Eq. (42) stands for imaginary part of a complex number.

Transmission of energy inside beam structure occurs only through the propagating modes. Time-averaged value of the energy flux associated with the mth propagating mode through the beam cross section is given by

$$I_m = \omega|A_m|^2\mathrm{Im}\left[\mathbf{f}_m^{\mathrm{T}}.\bar{\mathbf{q}}_m\right] \tag{43}$$

The percentage error in energy balance, on the other hand, can be defined as

$$\varepsilon = \left|\frac{1}{I^{\mathrm{in}}}\left[I^{\mathrm{in}} - \sum_{m=1}^{M_{\mathrm{p}}} I_m\right]\right| \times 100 \tag{44}$$

where M_{p} is the total number of propagating modes. As per the principle of energy conservation, the value of ε needs to be zero. Since propagation of wave does not require imposition of any boundary conditions, above check has been employed to assess numerical accuracy of solution procedure developed.

3. Numerical investigations

Numerical method presented in this work for propagation of wave and the evaluation of Green's function in a reinforced concrete beam takes into account the three-dimensional effect in an efficient manner. Computer programs have been written in FORTRAN-90 language to analyze these problems. These programs have been validated by comparing the obtained results with those available in the literature. An example of a homogeneous isotropic rectangular plate has been considered to validate the wave propagation formulation and program by comparing the obtained results for an isotropic rectangular beam cross section with those presented by Taweel et al. (2000). On the other hand, results presented by Zhu et al.

(1995) for plane strain problem in a 35-layer cross ply laminated composite plate have been considered to validate Green's function formulation and program. The normalized frequency, Ω, and normalized complex wave number, ζ, in case of plane strain problem have been defined by following expressions

$$\Omega = \frac{\omega H_{p}}{\sqrt{(C_{55}/\rho)_{0^{\circ}}}}; \quad \zeta = \lambda H_{p} \tag{45}$$

where H_{p} is the total thickness of laminated plate, ρ is the mass density and C_{55} is the shear modulus of rigidity of 0° lamina respectively.

Program developed for analysis of three-dimensional wave propagation organizes all the eigenvalues (wave numbers λ) so as to have propagating modes in ascending order followed by non-propagating modes in ascending order of their imaginary part. This arrangement has been found to be quite useful in selecting modes for superposition in Green's function solution.

Further, following expressions have been employed for the normalized frequency, Ω, and the normalized complex wave number, ζ, for the three-dimensional problem.

$$\Omega = \frac{\omega H}{\sqrt{(\mu/\rho)_{c}}}; \quad \zeta = \lambda H \tag{46}$$

Here H is the total depth of RC beam section, ρ is the mass density and μ is the shear modulus of rigidity of concrete, respectively.

Green's functions have been evaluated for typical T-shaped and L-shaped beams, which are commonly used in Civil Engineering structural systems. Basic assumption of elastic behaviour and homogeneous isotropic nature of concrete has been maintained in modeling the concrete section. Effect of stirrups has been neglected for simplicity and the longitudinal steel reinforcement bars have been modeled by square elements of equivalent cross sectional areas. Effect of corrosion of steel reinforcement bars has been modeled keeping in view the phenomenon of corrosion. The rust formed after corrosion of bars is known to expand in volume. This volume increase leads to development of micro-cracks in surrounding concrete and subsequent reduction in modulus of elasticity of concrete. It has been considered in the present study that corrosion of reinforcement steel bar produces a layer of rust, which is almost twice its original volume. The steel rust has been assumed to have 10% of modulus of elasticity of original steel and a negligible Poisson's ratio. Further, it has been assumed that the volume expansion of steel rust generates micro-cracks in surrounding concrete portion leading to reduction in its modulus of elasticity by 50%. Volume of this degenerated concrete has been considered to be six times the area of corroded steel reinforcement bar. With these reasonable assumptions, some useful investigations of corroded T and L beam sections have been performed. Brief discussion on the examples considered has been presented next. Effect of corrosion has been investigated with the help of displacement variation curves obtained from Green's function for original as well as corroded beams. A 9-node lagrangian element has been used to model reinforced concrete beam sections. The circular reinforcement bars have also been modeled by rectangular 9-node elements with equivalent cross sectional areas to reduce modeling complexities. In the present study, maximum mesh size employed for modeling a beam cross section included 1117 nodes for L-beam section with corrosion of re-bars.

Different examples solved here consider unit load acting at a particular point on the surface of the reinforced concrete beam while deriving Green's function. However, if required a line load with a known time-history can be applied by small modification in the program.

Example 1. Wave propagation in homogeneous, isotropic cylinder with rectangular cross section, Poisson's ratio = 0.3, and height to width ratio $H/W = 0.5$ has been considered. Symmetry conditions have been employed in both the directions and the quarter section of the beam has been modeled with
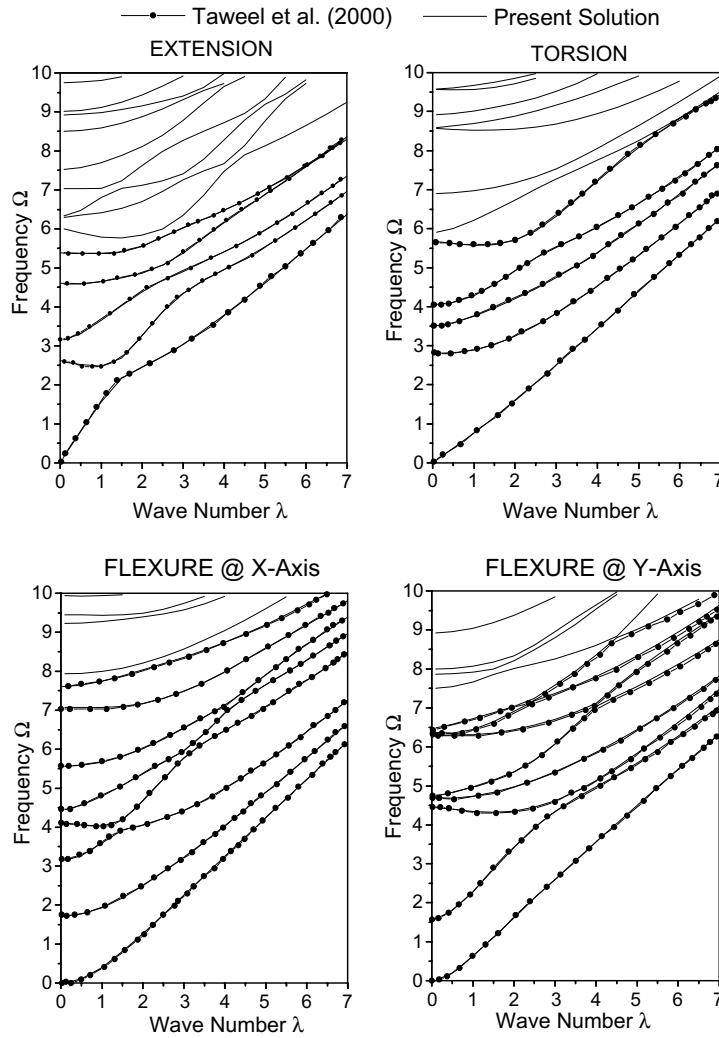
Fig. 2. Comparison of results for wave propagation in a beam of rectangular cross section with the results presented by Taweel et al. (2000).

8-noded quadrilateral elements forming a finite element mesh consisting of 65 nodes and 16 elements. Results obtained by the present method have been compared with those presented by Taweel et al. (2000) in Fig. 2. It can be observed from Fig. 2 that results of the present method correlate well with the published

Table 1
Elastic properties of 0° and 90° graphite/epoxy laminate in Example 2

Lamina (degrees)	C_{11} (GPa)	C_{33} (GPa)	C_{13} (GPa)	C_{55} (GPa)
0°	160.73	13.92	6.44	7.07
90°	13.92	13.92	6.92	3.50
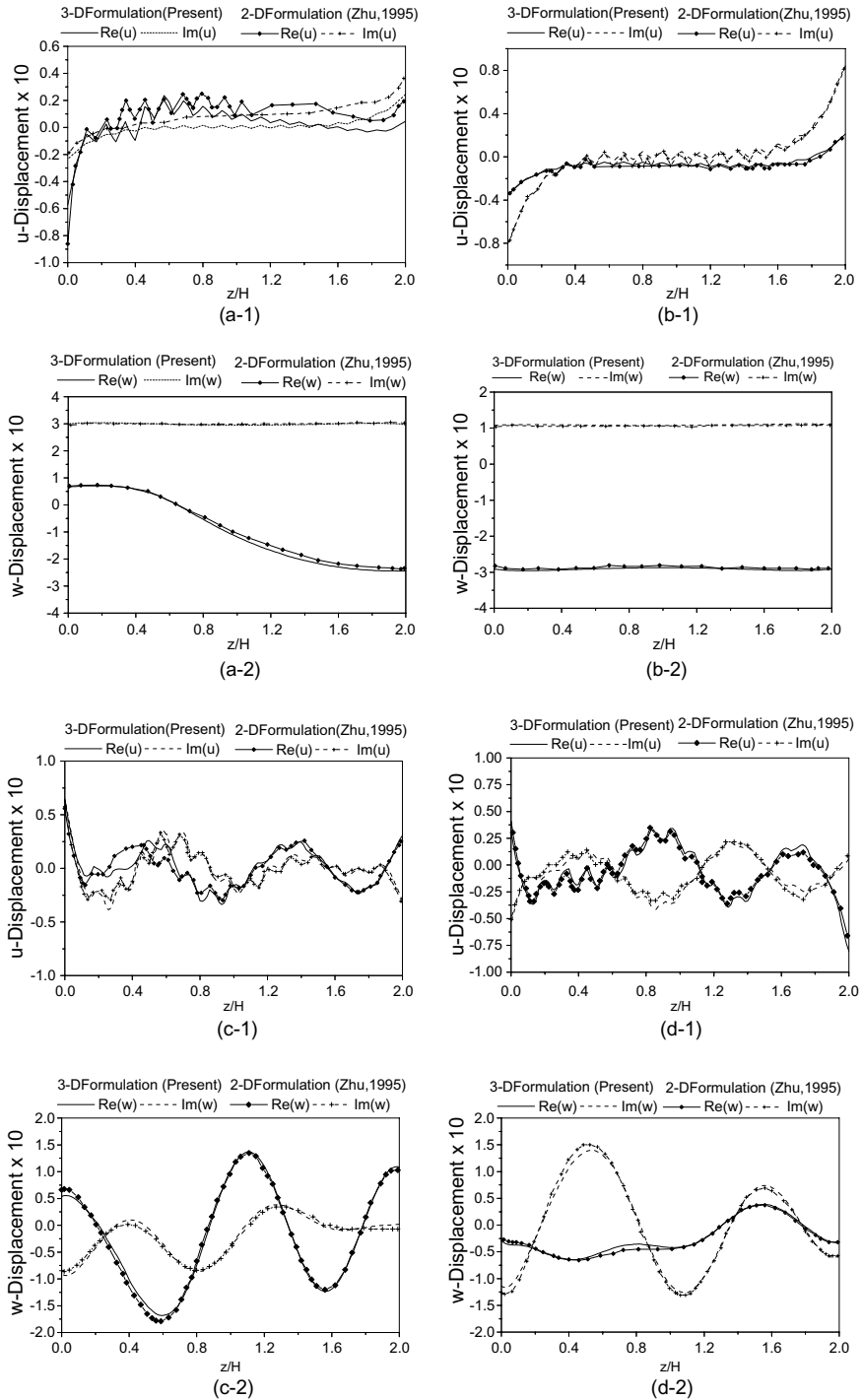
Fig. 3. The normalized horizontal and vertical displacements (*u, w*) for a 35 layer graphite epoxy plate at section (a) $x = 0.2H$, $\Omega = 1$; (b) $x = 10H$, $\Omega = 1$; (c) $x = 0.2H$, $\Omega = 10$ and (d) $x = 10H$, $\Omega = 10$.

results. Thus, it can be concluded that methodology and program presented here can be used for wave propagation in beams of finite width.

Example 2. A 35 layer $(90°/0°/\ldots90°/0°/90°/\ldots0°/90°)$ symmetric cross-ply laminated plate has been considered to validate the formulation of the Green's function. Elastic properties of $0°$ and $90°$ laminae are presented in Table 1. Plate of unit width has been considered to simulate the plane strain situation with the three-dimensional wave propagation program and boundary conditions are specified at all the nodes to restrain displacement in the width direction. The beam cross section of unit width has been descritized into 70 nine-noded elements in the thickness direction for consistency in comparing results of the Zhu et al. (1995), where an infinite plate was divided into 70 sub-layers. The unit load acting at a distance of $16H/35$ ($2H$ being thickness of plate) from top surface of the laminated plate has been considered to evaluate the Green's function at normalized frequencies $\Omega = 1$ and $\Omega = 10$. The horizontal and the vertical displacements along the cross section of the beam at distances $0.2H$ and $10H$ have been presented in Fig. 3(a)–(d) to highlight differences in the near as well as the far field effects. Comparison of results obtained by the present method with those by Zhu et al. (1995) shown in Fig. 3 validates the solution technique adopted for Green's functions problem in laminated composite beams. As a numerical check for accuracy, the percentage error in energy balance was calculated and it was found to be less than 1.5% in all the examples considered herein.

Example 3. A reinforced concrete T-beam with reinforcement and geometrical details shown in Fig. 4(a) has been considered. Details of finite element modeling of steel bar affected by corrosion and surrounding degenerated concrete portion has been presented in Fig. 4(b). Material properties for concrete, steel reinforcement and layers of rust and degenerated concrete around reinforcement bar have been presented in Table 2. Symmetry conditions have been utilized to model the cross section of the T-beam. Finite element
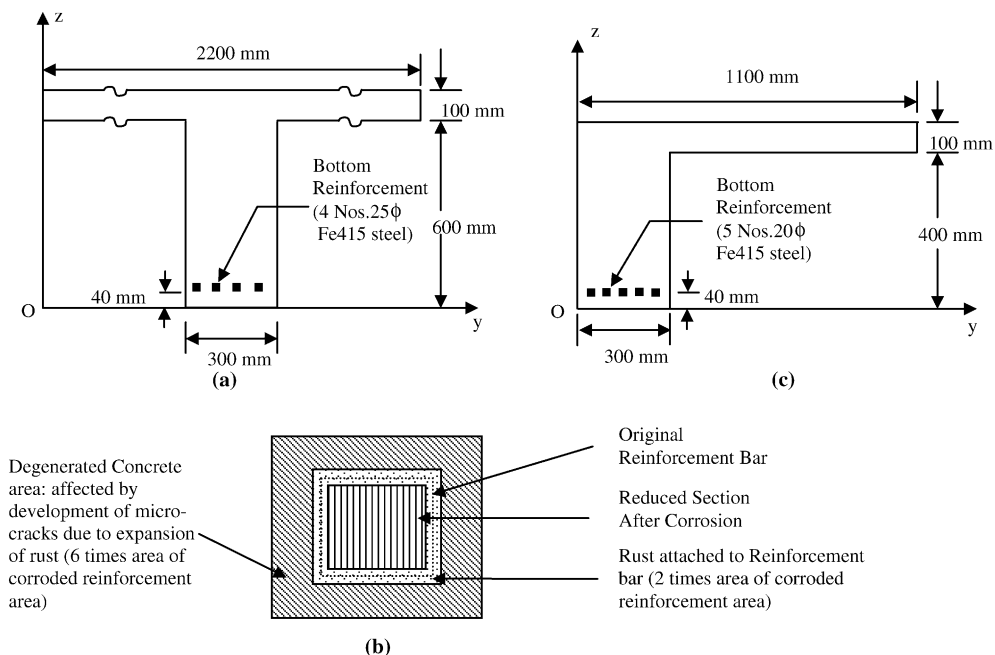

Fig. 4. Cross sectional dimensions of a reinforced concrete (a) T-beam; (b) enlarged view of conceptual model of cross section of a steel reinforcement bar affected by corrosion; and (c) L-beam cross section.

Table 2
Elastic properties of concrete, steel, rust due to corrosion and degraded concrete around rusted steel bar in reinforced concrete beams investigated in Examples 3 and 4

Material	C_{11}	C_{33}	C_{13}	C_{55}	Mass density (ρ) (kg/m^3)
Concrete	27.77 kPa	27.77 kPa	6.944 kPa	10.416 kPa	2500
Steel	277.2 GPa	277.2 GPa	12.45 GPa	76.33 GPa	7850
Rust	20.0 GPa	20.0 GPa	0.202 GPa	9.90 GPa	981.25
Degenerated concrete	13.88 kPa	13.88 kPa	3.472 kPa	5.208 kPa	2500

meshes with increasing order of refinement were employed to model the cross section till a converged solution was obtained. Dispersion curves for the T-beam with and without reinforcement are shown in Fig. 5(a) and (b). Finite element mesh with 303 nodes and 62 elements in half cross section was found to give converged solution for the T-beam without reinforcement. On the other hand, a similar mesh with 341 nodes and 69 elements in half cross section produced a converged solution for the T-beam with reinforcement. The Green's function for the T-beam need the wave propagation solution for the complete cross section. The T-beam sections with and without reinforcement were analyzed for the normalized frequency $\Omega = 1$ using finite element mesh of 519 nodes, 110 elements for full section of T-beam without reinforcement and 589 nodes, 123 elements for full section of reinforced T-beam. Eight propagating modes were found for $\Omega = 1$ in both types of T-beam sections. Green's functions have been obtained for a unit load acting on the top surface at a distance $y = W_f/2$, W_f being the width of the T-beam flange. The Green's functions have been evaluated for unreinforced and reinforced T-beam by considering 1200 modes. Through thickness displacement variations at locations ($x = H, y = W_f/2$) and ($x = 10H, y = W_f/2$) have been presented in Fig. 6(a-1) through (d-3). Above-mentioned reinforced concrete T-beam section affected by corrosion causing 10% reduction of reinforcement was considered next. Since effect of corrosion has been included for
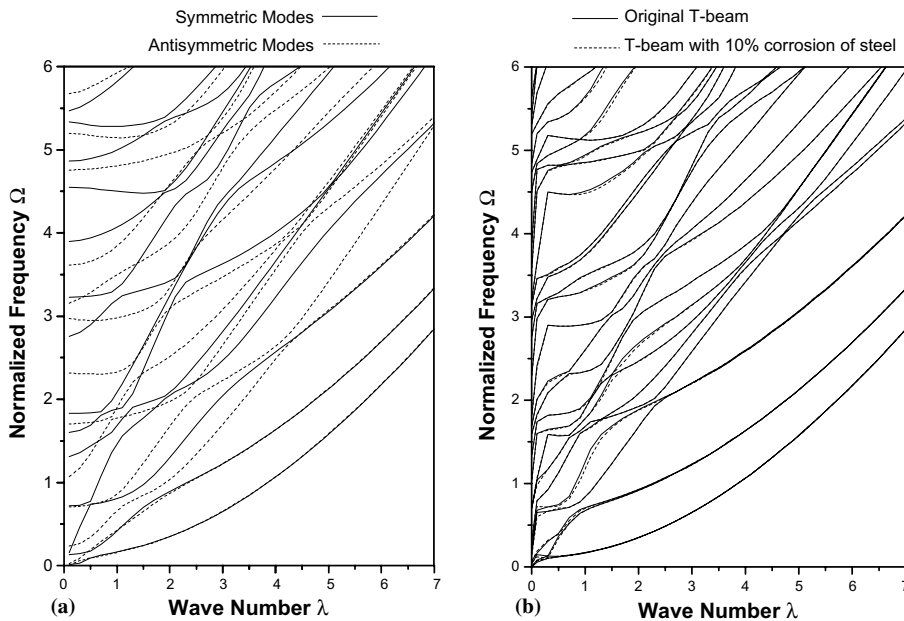

Fig. 5. Dispersion curves for (a) unreinforced and (b) reinforced T-beam (original and with 10% corrosion of steel).

modeling corroded beam section, a finite element mesh containing 1157 nodes and 255 elements was required to produce a converged solution. Dispersion curves for original reinforced T-beam and T-beam with 10% corrosion of steel have been compared in Fig. 5(b). Remarkable differences are observed in dispersion curves of these two forms of T-beam and it shows that corrosion can be identified through study of dispersion curves.

The axial displacement component in the unreinforced and the reinforced T-beam has been found to vary linearly. Comparison of curves in Fig. 6(a-1) through (b-3) indicates that the axial displacement
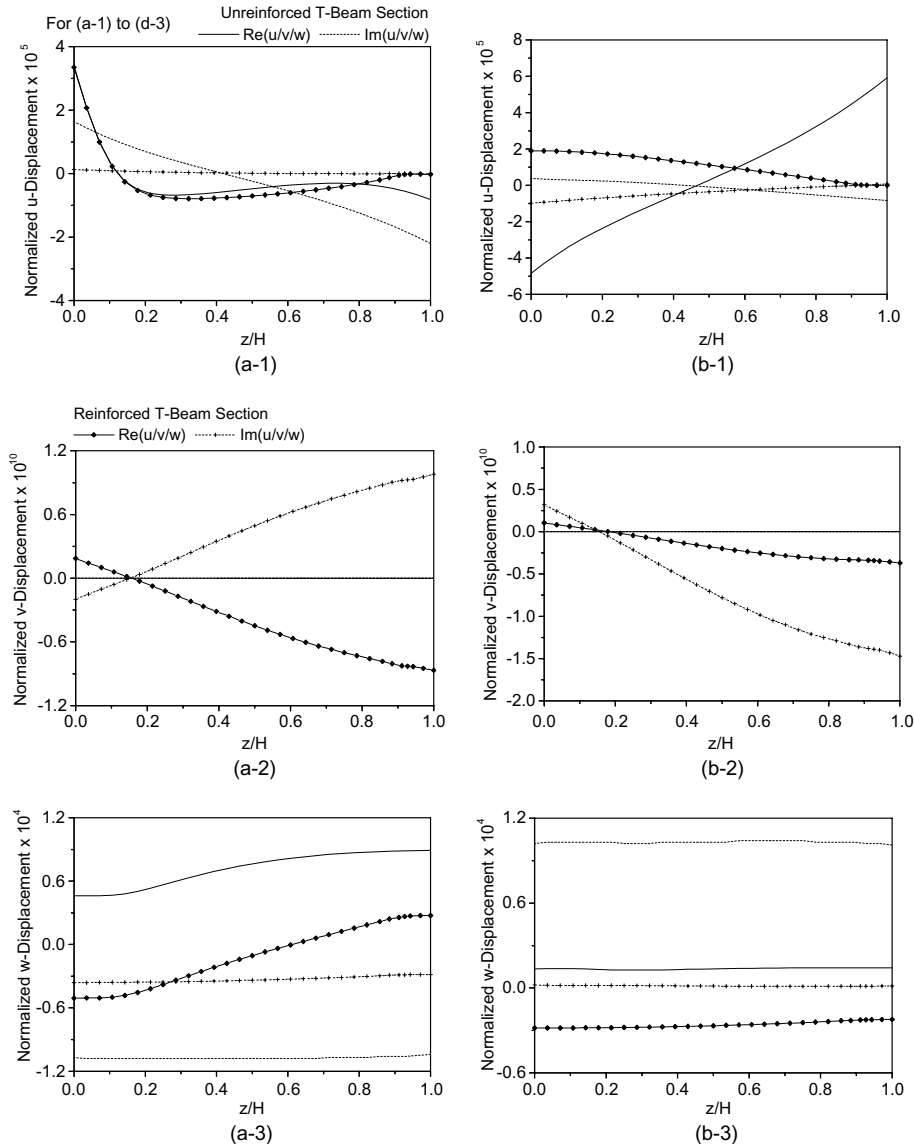
Fig. 6. Displacements u, v, w along thickness direction and at $y = W_f/2$ for unreinforced T-beam at section (a) $x = 0.2H$, $\Omega = 1$; (b) $x = 10H$, $\Omega = 1$; and for reinforced T-beam (and reinforced T-beam with 10% corrosion of steel) at section (c) $x = 0.2H$, $\Omega = 1$; (d) $x = 10H$, $\Omega = 1$.
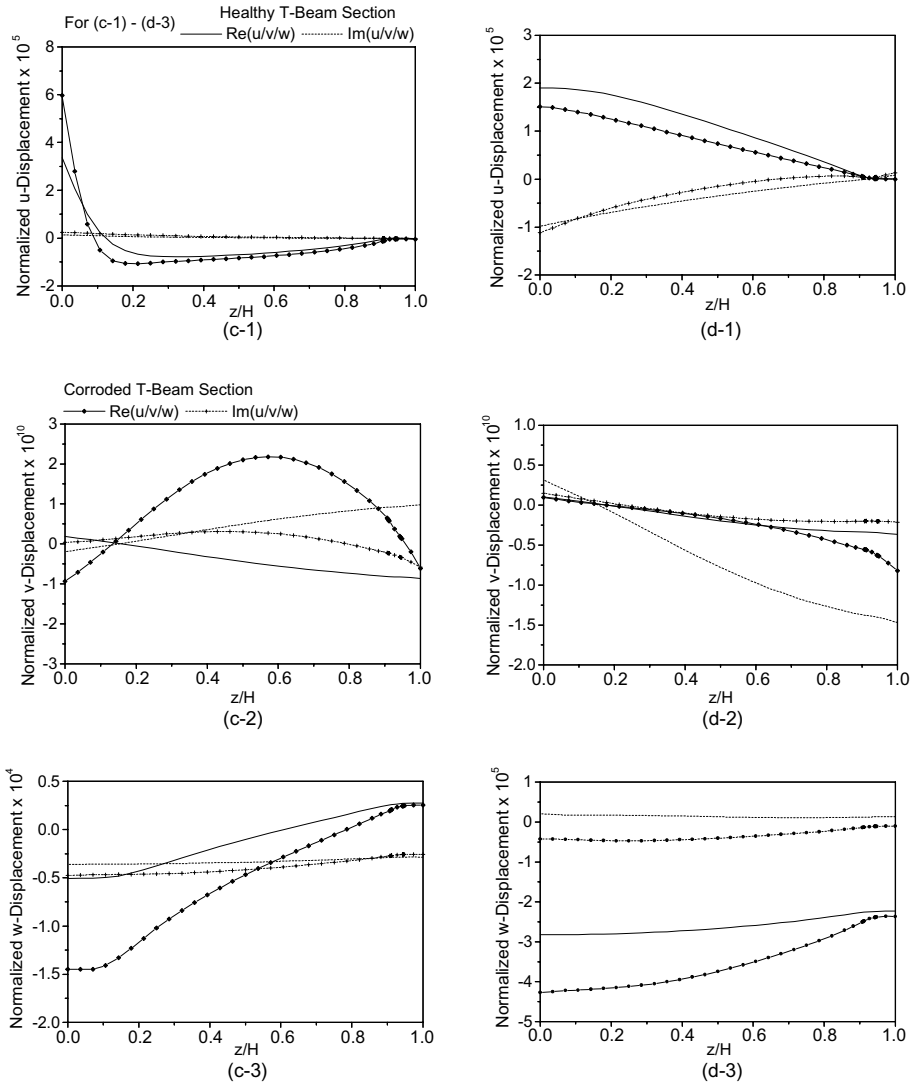
Fig. 6 (*continued*)

component for unreinforced and reinforced sections exhibit minor variations in near field. On the other hand, there is large difference in magnitudes. Further, patterns of the axial displacements of unreinforced and reinforced beam are opposite to each other in the far field. The transverse vertical displacement along thickness direction has been found to be the most predominant displacement in all the cases. The real part of the vertical displacement has been found to vary linearly for both unreinforced as well as reinforced T-beams. On the other hand, the imaginary part of the vertical displacement is observed to remain constant over the thickness for both unreinforced as well as reinforced T-beams. Nature of variation of the vertical displacement curves for unreinforced and reinforced sections was found to be almost identical. Inclusion of reinforcement in the T-beam is observed to affect vertical displacement component in different ways. The real part of the vertical displacement for reinforced T-beam diminishes in both near and far field regions

as compared to displacement variation for unreinforced beam. However, the imaginary part reduces in near field region and increases in far field region.

A reinforced T-beam affected by corrosion causing with 10% reduction of steel area has been analyzed by evaluating Green's function and similar displacement variation curves have been superimposed on those presented for the healthy reinforced T-beam section in Fig. 6(c-1) through (d-3). Comparison of these displacement curves indicates that both axial and vertical displacement components evaluated in the far field vary substantially and can be utilized for detection of corrosion. Further, the energy carried by the propagating modes has been evaluated for different cases and the percentage error in energy balance has been observed to be very low in all cases with maximum error being a mere 1.31% occurring for corroded reinforced T-beam. Accuracy of the numerical technique developed for Green's functions has thus been established.

Surface displacements are often easier to measure in experimental works. Comparison of surface displacements for healthy and corroded T-beam sections has been shown in Fig. 7(a)–(c). Axial surface displacement component compared in Fig. 7(a) shows considerable differences in magnitude as well as variation and can be very useful in detection of corrosion. Large differences are observed in the transverse displacements compared in Fig. 7(b) but its magnitude being extremely small it may not help much in
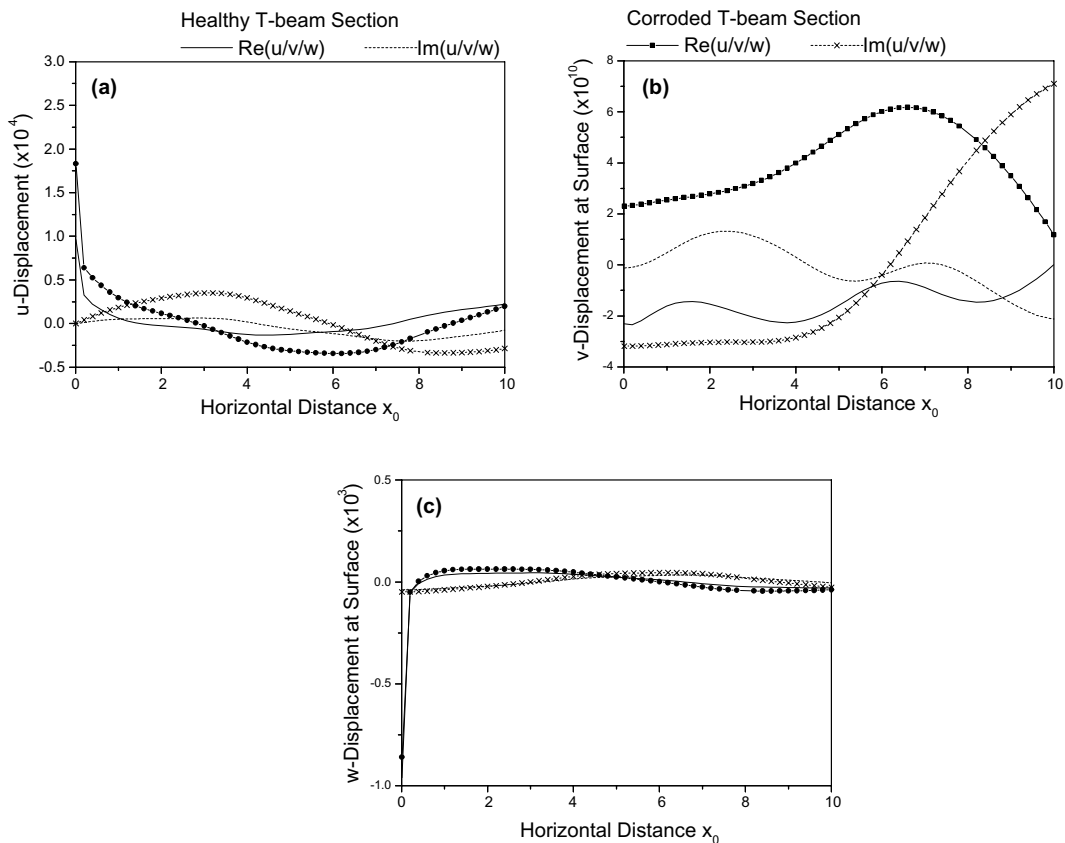

Fig. 7. Surface displacements at $y = W_f/2$ for reinforced T-beam (and reinforced T-beam with 10% corrosion of steel) along the top surface of the beam at $\Omega = 1$.

detecting corrosion effect. Vertical displacement component does not indicate much difference for healthy and corroded T-beam section.

Example 4. A reinforced concrete L-beam with reinforcement and geometrical details shown in Fig. 4(c) has been considered. Concrete of grade M25 and steel of type Fe415 are the constituent materials in the reinforced concrete L-beam under consideration and their material constants have been specified in Table 2. Dispersion curves for the L-beam with and without reinforcement have been presented in Fig. 8(a) and (b). A finite element mesh comprising of 335 nodes and 70 elements was found to be sufficient for providing converged solution for the L-beam without reinforcement. On the other hand, a marginally refined finite element mesh with 429 nodes and 89 elements was found to provide converged solution for the L-beam with reinforcement. The eigenvalues and eigenvectors corresponding to $\Omega = 1$ obtained using the converged sizes of finite element meshes have been utilized to evaluate the Green's function for unreinforced as well as reinforced L-beams. The number of propagating modes for unreinforced and reinforced L-beams has been found to be six for $\Omega = 1$. The unit load was applied on the top surface at a distance $y = H$. The Green's function was evaluated for unreinforced and reinforced L-beam by considering 1000 modes. Through thickness displacement variation curves at locations ($x = 0.2H, y = W_w/2$) and ($x = 10H, y = W_w/2$) have been presented in Fig. 9(a-1) through (d-3), where W_w represents the width of the web portion of the L-beam. The reinforced concrete L-beam section affected by corrosion causing 10% reduction of reinforcement has also been considered. A finite element mesh with 1117 nodes and 249 elements has been used to model the corroded section as explained by Fig. 4(b). Minor differences especially in the higher frequency range have been observed in dispersion curves of these two forms of L-beam and it can be quite useful to study dispersion curves while identifying corrosion in this type of RC beams.
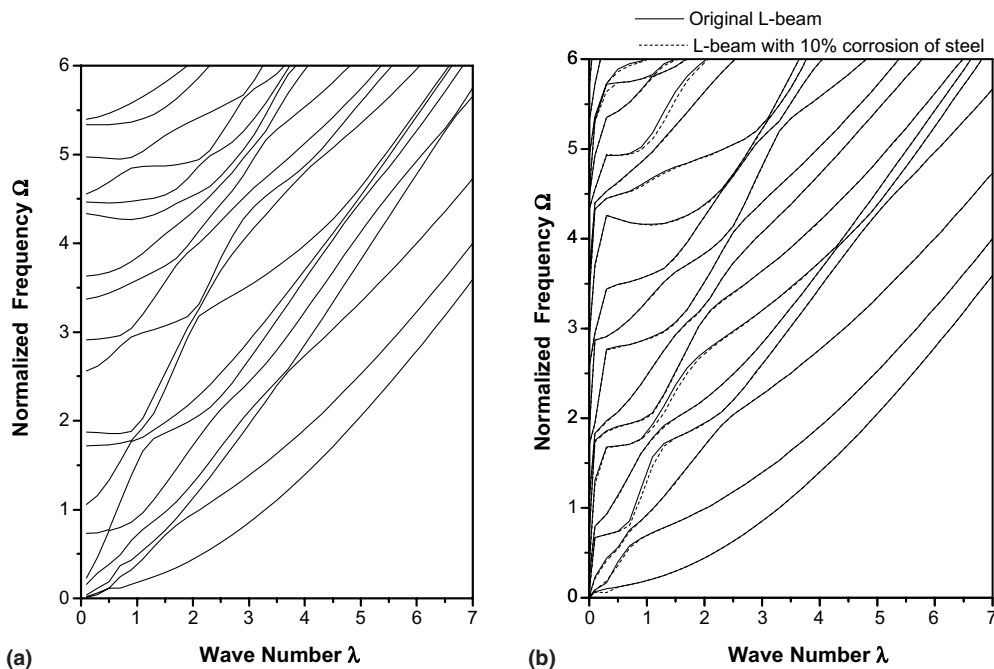

Fig. 8. Dispersion curves for (a) unreinforced, and (b) reinforced L-beam (original and with 10% corrosion of steel).

Displacement variation curves for unreinforced and reinforced L-beam are compared in Fig. 9(a-1) through (b-3). Displacements along the width direction have been found to be predominant for both unreinforced as well as reinforced L-beams. The lateral displacement component for the reinforced L-beam has been observed to reduce substantially as compared to the unreinforced L-beam. Changes in the vertical displacement variation curves for unreinforced and reinforced L-beams were observed to be of large magnitude in near field. Their variation patterns were observed to be of opposite nature for real and imaginary
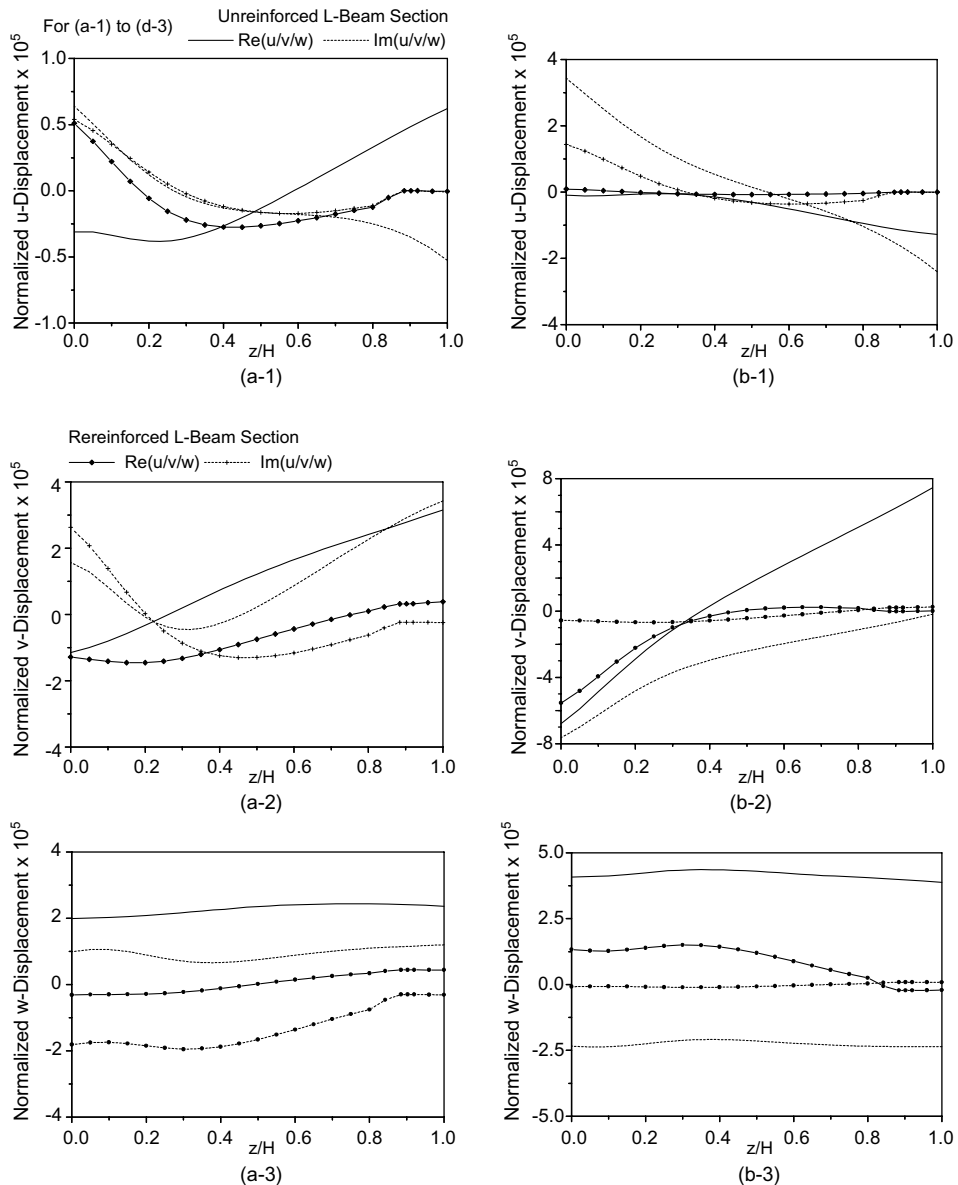

Fig. 9. Displacements u, v, w along thickness direction and at $y = 0.3H$ for unreinforced L-beam at section (a) $x = 0.2H$, $\Omega = 1$; (b) $x = 10H$, $\Omega = 1$; and for reinforced L-beam (and reinforced L-beam with 10% corrosion of steel) at section (c) $x = 0.2H$, $\Omega = 1$; (d) $x = 10H$, $\Omega = 1$.
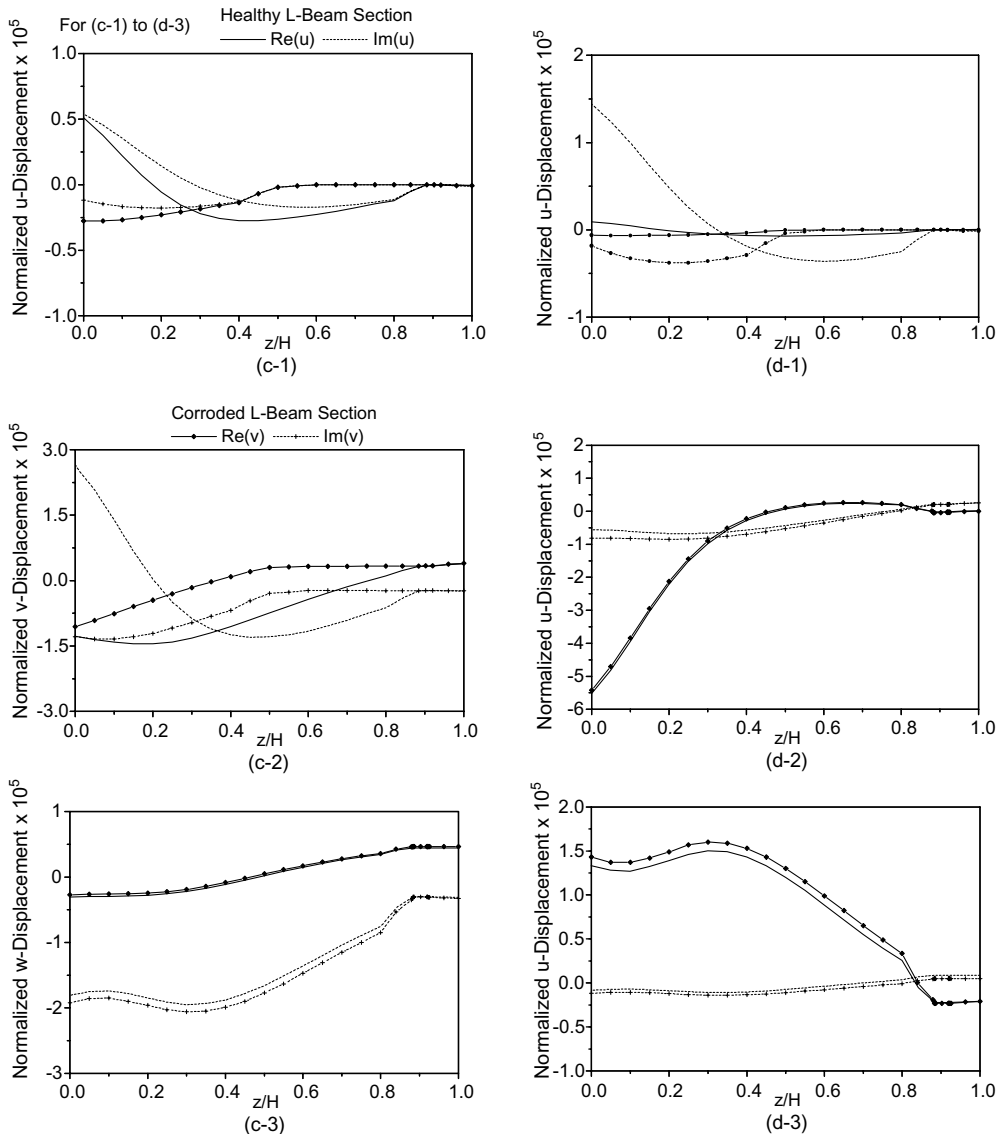
Fig. 9 (*continued*)

parts. The axial displacement component, on the other hand, did not indicate much change due to inclusion of reinforcement in the L-beam. Its variation changed from parabolic to linear. All the displacement components have been found to have negligible values in the bottom portion containing steel reinforcement for the reinforced L-beam.

A comparative study was performed to investigate effect of corrosion in the reinforced L-beam. Green's function was evaluated for the reinforced L-beam with 10% loss of steel caused by corrosion. Through thickness displacement variation curves for this corroded L-beam have been superimposed on the corresponding graphs obtained for the reinforced L-beam without any corrosion in Fig. 9(c-1) through (d-3). The axial displacement component in near field region and transverse displacement components evaluated
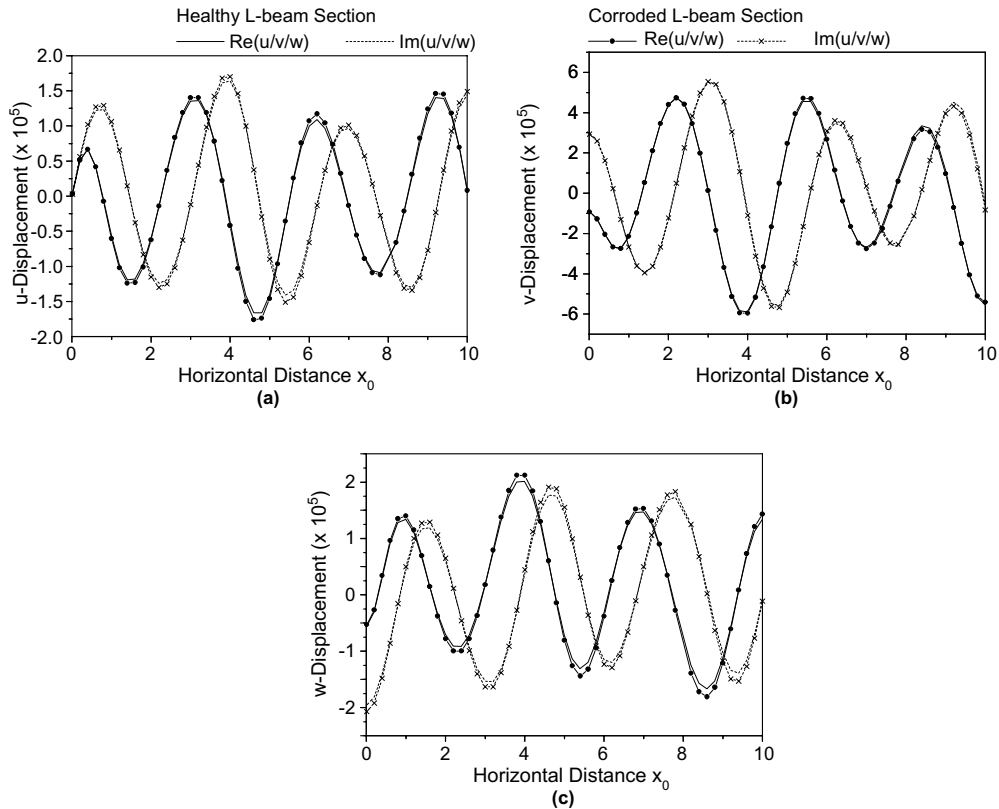
Fig. 10. Surface displacements at $y = 0.3H$ reinforced L-beam (and reinforced L-beam with 10% corrosion of steel) along the top surface of the beam at $\Omega = 1$.

in near and far field regions have been observed to vary substantially for corroded beam and these can be used effectively for detecting corrosion in reinforced L-beam section. Accuracy of the numerical method developed for the Green's function analysis was established by observing less than 1.5% error in both types frequencies considered for L-beam section.

Surface displacements have also been plotted for healthy and corroded L-beam sections in Fig. 10(a)–(c). Axial surface displacement component compared in Fig. 10(a) shows marginal difference in magnitude in far field region and similar observations are made for transverse displacement component shown in Fig. 10(b). Finite differences in magnitude of vertical displacement component are observed in far field region for healthy and corroded L-beam section, but the magnitude of displacement being very small it may not help much in identifying corrosion in field conditions.

Perceptible differences observed in through thickness displacement variation curves and some marginal differences in surface displacement curves for healthy and corroded L beam section indicate that measurement of displacements on the vertical face of L beam may be practically more useful for identifying corrosion with this technique.

4. Conclusions

A semi-analytical method for three-dimensional (3D) wave propagation analysis of reinforced concrete beam with arbitrary cross section has been presented. A solution procedure to evaluate 3D Green's function

for a general beam has been formulated by employing eigenvalues and eigenvectors evaluated beforehand from the dispersion equation of the beam for a particular excitation frequency. Green's function for an infinite cross-ply laminated plate has been evaluated using the 3D procedure presented here and the results compare well with the published analytical method. Further, 3D Green's function has been evaluated for practical cases of T-shaped and L-shaped reinforced concrete (RC) beams. Displacement variations in near as well as far fields at the normalized frequency of 1 have been presented to investigate response of unreinforced and reinforced concrete beams. For T-beam, axial and vertical displacement components whereas for L-beam axial and transverse displacement components have been found to show contrasting differences for healthy and corroded reinforced concrete beams. Surface displacement curves plotted for different RC beams have been observed to indicate some minor differences for corroded beams and may not be useful in detecting corrosion. Displacements measured on the vertical faces of RC beams will be of more relevance in detection of corrosion. Accuracy of the procedure has been established by observing negligible values of percentage error in input energy due to the unit excitation force and the output energy carried by the propagating modes. Green's function solution procedure developed here can be utilized as an effective tool for detecting corrosion in RC beams.

Acknowledgement

References

Cavigila, G., Morro, A., 2000. Wave propagation in multilayered anisotropic solids. International Journal of Engineering Science 38 (8), 847–863.

Chimenti, D.E., 1997. Guided waves in plates and their use in materials characterization. ASME Applied Mechanics Review 50 (5), 247–284.

Datta, S.K., Shah, A.H., Bratton, R.L., Chackraborty, T., 1988. Wave propagation in laminated composite plates. Journal of the Acoustical Society of America 83, 2020–2026.

Green, E.R., Green, W.A., 2000. A computational method for wave propagation from a point load in an anisotropic material. Ultrasonics 38, 262–266.

Karunasena, W.M., Shah, A.H., Datta, S.K., 1991. Wave propagation in a multilayered laminated cross-ply composite plate. Transactions of the ASME Journal of Applied Mechanics 58, 1028–1032.

Liu, G.R., Tani, J., Watanabe, K., Ohyoshi, T., 1990. Harmonic wave propagation in anisotropic laminated strips. Journal of Sound and Vibrations 139 (2), 313–324.

Liu, G.R., Lam, K.Y., 1996. Two-dimensional time-harmonic elastodynamic Green's functions for anisotropic media. International Journal of Engineering Science 34 (11), 1327–1338.

Mal, A., 2002. Elastic waves from localized sources in composite laminate. International Journal of Solids and Structures 39, 5481–5494.

Mukdadi, O.M., Datta, S.K., 2003. Transient ultrasonic guided waves in layered plates with rectangular cross-section. Journal of Applied Physics 93 (11), 9360–9370.

Mukdadi, O.M., Desai, Y.M., Datta, S.K., Shah, A.H., Niklasson, A.J., 2002. Elastic guided waves in a layered plate with rectangular cross section. Journal of the Acoustical Society of America 112 (5), 1766–1779.

Taweel, H., Dong, S.B., Kazic, M., 2000. Wave reflection from the free end of a cylinder with an arbitrary cross-section. International Journal of Solids and Structures 37, 1701–1720.

Zhu, J., Shah, A.H., Datta, S.K., 1995. Modal representation of two-dimensional elastodynamic Green's functions. Journal of Engineering Mechanics 121 (1), 27–36.

Zhuang, W., Shah, A.H., Dong, S.B., 1999. Elastodynamic Green's function for laminated anisotropic circular cylinders. Transactions of the ASME Journal of Applied Mechanics 66, 665–674.